Title
DOSIMETRY OF n MESONS USING SILICON DETECTORS AND PLASTIC SCINTILLATORS

Authors
Raju, M.R.
Lampo, E.
Curtis, S.B.
et al.

Publication Date
1969-08-01

Submitted to Physics in Medicine
and Biology

UCRL-19340
Preprint

DOSIMETRY OF π MESONS USING SILICON DETECTORS AND PLASTIC SCINTILLATORS

M. R. Raju, E. Lampo, S. B. Curtis,
and C. Richman

August 1969

AEC Contract No. W-7405-eng-48

LAWRENCE RADIATION LABORATORY
UNIVERSITY of CALIFORNIA BERKELEY

DISCLAIMER

Dosimetry of π Mesons Using Silicon Detectors and Plastic Scintillators

M. R. Raju, E. Lampo, S. B. Curtis, and C. Richman

Lawrence Radiation Laboratory, University of California, Berkeley, California, and University of Texas at Dallas

August 1969

Abstract. The dosimetry of both π^+ and π^- beams, with use of semiconductor detectors and plastic scintillators, is described. Depth-dose distributions, isodose distributions, and integral and differential range curves are presented. By use of a time-of-flight system the dosimetric information for a pure pion beam is obtained. The muon and electron contamination reduce the peak-to-plateau ratio. Pion beams of low energy give better depth-dose distributions. Nearly 50% of the dose at the peak of the depth-dose distribution of a π^- beam is found to be due to nuclear events.

1. Introduction

The dose delivered by a π^--meson beam increases slowly with depth, giving rise to a sharp maximum, (known as the Bragg peak), near the end of the range. This is like the behavior of other heavy charged particles. When the π^- mesons stop in the medium, they are captured by the constituent nuclei. The captured nuclei explode into short-range and heavily ionizing fragments, which enhance the dose at the peak. This may have a radiotherapeutic application because these

highly ionizing fragments are effective in decreasing radioresistance of hypoxic cells in a tumour. This idea was informally suggested by a few people, including one of the authors (C. R.), as early as 1952, but detailed calculations by Fowler and Perkins (1961) generated heightened interest in the use of π^- mesons for radiotherapy. Biophysical experiments have been carried out in this Laboratory over the last six years (Raju, Aceto, and Richman 1965, Richman, Aceto, Raju, and Schwartz 1966, Raju, Lampo, Curtis, Sperinde, and Richman 1967a, Raju, Richman, and Curtis 1967b, Curtis and Raju 1968, Richman, Raju, and Schwartz 1967, Loughman, Feola, Raju, and Winchell 1968, Feola, Richman, Raju, Curtis, and Lawrence 1968, Raju, Amer, Gnanapurani, and Richman 1969). Some physical measurements were also made at CERN, Switzerland, and at Brookhaven National Laboratory (Goebel 1966, Baarli 1967, Sullivan and Baarli 1968, Tisljar-Lentulis 1966). This paper describes the technique used in pion dosimetry and the results obtained by using semiconductor detectors and plastic scintillators.

2. Production of Pion Beams

Pions can be produced in a nuclear interaction by any strongly interacting particle if its energy is great enough. They are generally produced by a primary beam of protons. Our experiments at Berkeley are carried out at the 184-inch synchrocyclotron. This machine provides an accelerated beam of 732-MeV protons that strike a 5-cm-thick beryllium target in their outer orbit and produce neutral, positive, and negative pions. The experimental arrangement is shown in Fig. 1. The π^- are deflected out of the cyclotron by the cyclotron fringe field, and after leaving the

cyclotron tank through a window, enter a small quadrupole focusing magnet (meson quad), then travel along a channel (dashed line in fig. 1) through the main cyclotron shielding (hatched area). The pions then enter the meson cave, where various arrangements of magnets are used for energy selection and for focusing the beam. A bending magnet is used for momentum selection. The cyclotron produces pions in a range of energies from 0 to about 450 MeV (the upper limit being determined by the energy of the primary proton beam). In the change from a π^- beam to a π^+ beam, all the magnetic fields, including that of the cyclotron, are reversed. The magnetic-lens system remains unchanged for pions of the same energy, regardless of charge.

Neutral pions have a very short lifetime, $\approx 10^{-16}$ sec, and decay into two γ rays in the target. The γ rays are converted into electron-positron pairs that go mainly in the forward direction. The electrons with the same momentum as pions selected by the bending magnet constitute electron background in the beam.

Charged pions have a mean life of 2.54×10^{-8} sec. Hence some of them decay in flight into muons, and this constitutes the muon background in a pion beam.

The presently available π^- beams are too low in intensity for therapeutic applications.* The pion beam at the 184-inch synchrocyclotron at Berkeley is the most intense, being 10^6 particles/sec. In terms of dose rate, it is ≈ 0.5 rad/min over an area of 3×5 cm^2. With such a

*Machines that will produce pion intensities nearly two orders of magnitude higher than the one presently available are under construction at Los Alamos Scientific Laboratory; Vancouver, Canada; and Zürich, Switzerland.

beam, however, physical measurements can be carried out quite well.

3. Experimental Technique

The characteristics of the pion beam as it passes through an absorbing medium of Lucite, and the energy distribution of π^- stars in silicon obtained by using lithium-drifted silicon detectors, have been reported (Raju, Aceto, and Richman 1965). The energies deposited in the detector where pions stop and produce stars have been found to extend beyond 60 MeV. The silicon nucleus with its mass number 28 has α-particle structure, and hence the nuclear interaction when π^- mesons stop in silicon may not be significantly different from that in other alpha-structure nuclei, such as carbon and oxygen, the main constituents of tissue. The depth-dose distribution, as measured by a silicon detector, is in good agreement with the calculated depth dose based on stopping π^- meson interactions in oxygen (Curtis and Raju 1968).

The dose deposited in the detector can be measured by integrating the charge liberated in the detector by ionizing radiations such as x and γ rays if the leakage current of the detector is annulled by using a balancing circuit (see Bailey and Kramer 1964). With energetic charged particles, however, radiation damage prevents their use at levels above that produced by the leakage current. In the present application these difficulties are alleviated by accepting only the ac pulses, and the pion beam intensity is not high enough to cause significant radiation damage.

The charge liberated in the lithium-drifted silicon detector is directly proportional to the energy deposited by the radiation. A charge-sensitive preamplifier yields a voltage pulse proportional to the energy

deposited in the detector, and these pulses are further amplified by a main amplifier. The leakage current of the lithium-drifted detectors is a few microamperes (depending on their thickness), and this current is quite comparable to the current generated in the detector due to pions passing through it. (The total pion intensity seen by the detector is about 5×10^4/sec). The detector leakage current is blocked by the ac amplification.

In our previous work, the amplifier output was integrated by using an analogue integrator (Raju, Lampo, Curtis, Sperinde, and Richman 1967a). The ac character of the signal necessitated the use of a polarity-clipping circuit (i.e., correcting the negative overshoot) before integration. This system had a linear energy range of 100 to 1. Pion beams are always produced with muon and electron contamination. For a beam of momentum 190 MeV/c, the most probable energy losses--in a 3-mm detector, for example--are 1 MeV by the electrons and 1.2 MeV by the pions; the energy lost by the muons is intermediate between these values (Raju, Aceto, and Richman 1965). There is considerable spread in energy losses due to Landau fluctuations (Landau 1944, Macabee, Raju, and Tobias 1968). At the end of the range the pions stop and produce stars, thereby depositing energies in the detector sometimes exceeding 60 MeV (Raju, Aceto, and Richman 1965). These high energy stars can be observed even with thin lithium-drifted silicon detectors (e.g., 1 mm) because a considerable portion of the star energy is deposited locally. However, in the region where the pion beam enters the medium (usually called the plateau region), the energy deposition in the detector is proportional to the thickness of the detector. The use of

a thin detector is advantageous for dose measurements, especially in the pion-stopping region, since this region could be small, for a narrow momentum spread of the primary π^- beam. This thin detector necessitates linearity over a wider energy range of the overall system. In our previous work, the linear range was only of the order of 100-fold; we were restricted to using a 3-mm-thick lithium-drifted silicon detector, and it was critical.

The linearity of the system has been improved considerably by changing to digital processing, using a 4096-channel analog-to-digital converter (ADC). The output of the linear-gated amplifier is stretched for compatibility before being fed to the ADC. The ADC translates the signal amplitude to a channel number of a 12-bit binary number. This code is fed to a digital on-line computer, which processes and stores the total number of particles and the total energy. In addition, the computer is also programmed to print out the pulse-height spectrum. The block diagram of the overall system and a photograph are shown in figs. 2 and 3 respectively. A pulse generator is used to calibrate the system and to check system linearity.

Our primary π^- beam is contaminated with 25% electrons and 10% muons. Since the semiconductor detector system is fast and measures the dose due to each particle, it is possible to measure the dose due to pions only, if the muons and electrons are resolved from the pions by using a time-of-flight system and gating the semiconductor detector system with the signal due to pions only.

The time-of-flight system (TOF) measures the time each beam particle takes to travel a fixed distance. Because of space restrictions

this length was only 17 feet in our system; increasing the path length would improve the resolution of the system. A plastic scintillation counter is placed at each end of the flight path. In a contaminated pion beam of a given momentum, muons and electrons travel faster than pions. The velocity spectrum of the particles, as expressed by the time delay between the two scintillation counter pulses, is processed via a time-to-pulse-height converter. The TOF pulse spectra which gate the semiconductor system for the contaminated and pure beams of π^- mesons, and the TOF pion signal, are shown in fig. 4.

The lithium-drifted silicon detector, housed in an electrically shielded Lucite box, can be remotely positioned in three axes in a water phantom. The data from the semiconductor detector are accumulated in the computer during the time it takes the monitor scintillator system to accumulate a fixed number of counts. Data are thus collected for each position of the detector in the water phantom.

In addition to the semiconductor detector system, plastic scintillators provide fast coincidence and anticoincidence gating in conjunction with the TOF system furnishing gating signals for obtaining integral range curves (number-distance curves) and differential range curves (numbers of particles stopped as a function of absorber thickness). The block diagram of such a setup is shown in fig. 5. Triple coincidence counts between plastic scintillators 1, 2 and 3 as a function of absorber thickness (normalized by the number of coincidence between 1 and 2) yield the number-versus-distance curve. Normalized triple coincidence between 1, 2 and 3 but with counter 4 in anticoincidence, produce the differential range curve. Integral and differential range information

for "pure" pion beams was obtained by employing the TOF system.

The cyclotron is pulsed 64 times per second, thus producing 64 coarse groups of pions per second. The mode of cyclotron operation can be controlled so that these groups of pions are spread out over either of two periods. The "short-spill" mode spills the beam over a period of approximately 400 μsec. It is also possible (by use of the auxiliary dee mechanism of the cyclotron) to spread each group of pions over a longer period of 8 to 10 msec. Even in this mode, roughly half of the total beam arrives during the first 400 μsec, producing a spike of beam intensity, and the remainder is stretched over 8 to 10 msec (Vale 1969). We use the stretched beam and gate off the system during the spike to prevent overloading of the electronic system, and thereby avoid the nonlinearities that would occur from saturation.

Because of beam-intensity fluctuations, two plastic scintillators connected in coincidence are used to monitor the beam (see fig. 2). The various integral and differential counts are collected during a preset number of monitor counts, thereby normalizing all measurements so that beam intensity fluctuations are unimportant.

4. Results and Discussion

4.1. Dose and number of particles as a function of depth in water

The linearity of the semiconductor detector system (including ADC) is checked with a calibrated pulser, and the system is found to be linear from 0.18 to 50 MeV. The energy threshold is set at 0.15 MeV,

thereby limiting measurement to energy depositions above this value. The range of linearity can be shifted by adjusting the gain in the main amplifier. This linear range is adequate for the detector thicknesses (1 to 3 mm) used in the investigation reported here.

By measuring the dose in a water container without water in it, the beam used is found to be slightly divergent. The intensity of the beam in air at a position where pions stop and produce stars in water is found to be 15% less than at the point of entrance, due to this divergence in the initial beam.

The depth-dose distribution of π^- mesons is measured by using lithium-drifted silicon detectors 1, 2, and 3 mm thick to determine which detector is most suitable for such measurements. The ratios of the dose at the peak to that at the entrance for the three detectors are found to be the same within the experimental accuracy. In addition, the energy depositied per π^- at the peak region is also found to be proportional to the thickness of the detector. These results indicate that the pion stars deposit energy over a finite range comparable to the thicknesses of the detectors used.

For the rest of the measurements, a lithium-drifted silicon detector 2 mm thick is used. As mentioned earlier, the computer printout gives the total number of particles passing through the detector as well as the total energy deposited by them. When the semiconductor detector system is gated by the TOF pion signal, data for essentially pure π mesons (without the muon and electron contamination) are obtained. The plots of the total number of particles passing through the detector and the total energy deposited by them as a function of depth

in absorber (water) give the integral range (also called number-distance) and the depth dose curves respectively. Figure 6 shows such curves, both for contaminated and for pure π meson beams of energy 65 MeV for the semiconductor detector.

Measurements are taken for a π^+ beam for comparison with the π^- results. Positive pions with the same momentum as π^- mesons can be produced by reversing the polarity of the whole magnetic system, including the field of the cyclotron.

The characteristic difference in interaction between π^+ and π^- mesons is at the ends of their ranges. When the π^+ meson comes to rest in a medium, the Coulomb repulsion keeps it from being captured in an atomic orbit. Instead, it decays into a muon with an energy of 4 MeV, which then decays into a positron with an energy distribution peaking around 30 MeV. Hence at the end of the range, the π^+ does not add much to the dose except for a small contribution due to the muon and positron.

The electron contamination in a π^+-meson beam is only around 10%, compared with 25% for a π^--meson beam, whereas the muon contamination is the same for both the beams. If a depth-dose distribution of pure beams of π^+ and π^- mesons, obtained by using the TOF gating of the semiconductor detector system, are compared, the difference can be attributed to the star events from π^- capture, except for the small contribution due to muons and positrons resulting from the π^+ decay.

In order to evaluate the dose contribution due to π^- stars, the depth-dose distributions of pure π^-- and π^+-meson beams of energy 65 MeV in water are measured; they are shown in fig. 7.

4.2. Differential and integral dose distribution

The differential and integral dose distributions can be computed from the measured pulse-height distribution at any point. The differential dose distribution gives the distribution of energy depositions in the detector, whereas the integral dose distribution gives the total energy deposited in depositions greater than a particular energy. The differential and normalized integral dose distributions at the peak of the π^- depth-dose curve are shown in fig. 8. The energy of a pion that has a range of 2 mm of silicon, the detector thickness used, is about 8 MeV. Hence energy depositions greater than 8 MeV are due to star events. As can be seen from the differential dose distribution, the area under the curve over an energy range of 0 to 8 MeV approximates the area under the curve above 8 MeV. Hence the dose contribution due to star events is about half of the total dose at the peak region of a depth-dose distribution for a π^- contaminated beam. The peak at 50 MeV in differential dose distribution is a saturation effect; any event depositing energies greater than 50 MeV is counted as 50 MeV.

Similarly, from the plot of the normalized integral dose distribution it is seen that the fraction of the dose due to energy depositions greater than 8 MeV--i.e., from the stars--is about 45% of the total.

The normalized integral dose distribution for pion beams at various depths are shown in fig. 9. The two curves for the π^- beam corresponding to the peak and halfway down the falling portion (trailing edge) of the depth-dose distribution are similar, thereby showing that the ionization density at the peak and thereafter is about the same. On the other hand, the curve corresponding to the point halfway up the rising portion

(leading edge) of the depth-dose curve falls below the other two curves. The ionization density at this point is considerably less. This is expected because the π^- mesons making stars at and beyond the peak of the depth-dose curve have to pass this point and hence deposit dose of lower ionization density. The dose fractions due to the star events in pure and contaminated π^- beam are 55 and 45 percent respectively. In the π^+ beam at the peak of the depth-dose curve, the dose fraction greater than 10 MeV is very small. The contribution above 8 MeV is due to the additional energy deposition from μ^+ and e^+ arising from the decay of π^+ near the end of the range.

4.3 Isodose contours

Isodose contours give a much clearer picture of the spatial dose distribution. Such curves can be constructed from a series of beam profiles taken in water at various depths. Figures 10 through 13 show such isodose contours for contaminated as well as for pure π^+ and π^- beams of energy 65 MeV in water. The distortion of the isodose contours is due to a slight nonuniformity in particle momentum laterally across the beam.

4.4 Depth-dose distribution of 90 MeV and 65-MeV π^- beams in Lucite

To minimize the effect of the divergence of the beam on the depth dose distribution, the detector position was fixed and the thickness of the Lucite absorber varied. With the same setup, the data for integral and differential range curves when plastic scintillators are used was also obtained and are presented in the next section. Figure 14 shows the depth-dose distribution of contaminated as well as pure π^- beams of energies 65 and 90 MeV. It can be seen that for the

pure 90-MeV π^- beam, the dose at the peak is not significantly different from the contaminated beam when compared with 65-MeV beam. This is because of less contamination in the 90-MeV π^- beam. The lower value of the peak-to-plateau ratio for the high energy beam is mainly due to loss of particles by nuclear attenuation and multiple scattering before reaching the end of the range.

4.5. Measurements of differential and integral range curves with plastic scintillators

Differential and integral range curves were obtained with the scintillator counter array. The block diagram of the scintillation counter systems for obtaining these curves simultaneously with the semiconductor detector system is shown in fig. 5. The integral range curves obtained with both the systems are found to be the same. The differential range curves--i. e., the number of particles stopping in the Counter 3 as a function of Lucite absorber thickness for pure and contaminated 90-MeV and 65-MeV π^- beams--are shown in fig. 15. Such curves are very useful in determining the depth at which most of the particles stop.

5. Conclusions

This series of experiments demonstrate the complexities in providing adequate dosimetric information for pion beams. In addition to the variation of dose with depth, there are significant differences in the quality of dose. Contamination not only reduces the peak-to-plateau ratio, but also increases the relative contribution of dose due to low-LET radiation. Low-energy π^- beams give higher peak-to-plateau ratios.

We are grateful to Dr. John H. Lawrence and Dr. Cornelius A. Tobias for continuing interest and encouragement. We thank Frederick S. Goulding, Lloyd B. Robinson, and Frank T. Upham for help in instrumentation. We are indebted to Kenneth M. Crowe for making his on-line computer available.

This work was done under auspices of the U. S. Atomic Energy Commission, the American Cancer Society, and the Office of Naval Research.

References

- Baarli, J., 1967, Rad. Res. Suppl. 7, 10.
- Bailey, N. A., and Kramer, G. (1964). Rad. Res. 22, 53.
- Curtis, S. B., and Raju, M. R. (1968), Rad. Res. 34, 239.
- Feola, J. M., Richman, C., Raju, M. R., Curtis, S. B., and Lawrence, J. H., 1968, Rad. Res. 34, 70.
- Fowler, P. H., and Perkins, D. H., 1961, Nature, 189, 524.
- Goebel, K., 1966, Z. Naturf. 21a, 1808.
- Landau, L., (1944). J. Phys. USSR, 8, 201.
- Loughman, W. D., Feola, J. M., Raju, M. R., and Winchell, H. S., 1968, Rad. Res. 34, 56
- Maccabee, H. D., Raju, M. R., and Tobias, C. A., (1968). Phys. Rev. 165, 469.
- Raju, M. R., Aceto, H., and Richman, C., (1965). Nucl. Inst. and Methods, 37, 152.
- Raju, M. R., Amer, N. M., Gnanapurani, M., and Richman, C., 1969, accepted for publication in Rad. Res.
- Raju, M. R., Lampo, E. J., Curtis, S. B., Sperinde, J. M., and Richman, C., (1967a). IEEE Trans. Nucl. Sci. NS-14, 559.
- Raju, M. R., Richman, C., and Curtis, S. B., (1967b). Proceedings of the First International Symposium on the Biological Interpretation of Dose from Accelerator Produced Radiation, held at the Lawrence Radiation Laboratory, Berkeley, California, March 13-16. Cont - 670305. Health and Safety TID-4500. p. 349.

- Richman, C., Aceto, Jr., H., Raju, M. R., and Schwartz, B., 1966, Am. J. Roentg. 96, 777.
- Richman, S. P., Richman, C., Raju, M. R., and Schwartz, B., 1967, Rad. Res. Suppl. 7, 182.
- Sullivan, A. H., and Baarli, J., 1968, Phys. Med. Biol. 13, 435
- Tisljar-Lentulis, G. M., 1966, Rev. Sci. Instr. 37 291.
- Vale, James T. (Lawrence Radiation Laboratory), private communication, 1969.

FIGURE LEGENDS

Fig. 1. Experimental setup for producing a π^- beam.

Fig. 2. Block diagram of the semiconductor setup.

Fig. 3. Photograph of the overall system.

Fig. 4. Time-of-flight spectrum of π^- beam:

o contamined beam,

ø pion spectrum used to gate the semiconductor detector and plastic scintillators.

Fig. 5. Block diagram of the plastic scintillator setup used to measure integral and differential range curves.

Fig. 6. Number-distance (integral range) curves and depth-dose distribution of 65-MeV π^- beam in water:

o pure pion beam,

△ contaminated beam.

Fig. 7. Depth-dose distribution of 65-MeV π^- and π^+ pure beams in water.

Fig. 8. Differential and integral dose distribution at the peak of the 65-MeV contaminated π^- beam:

o integral dose distribution,

△ differential dose distribution.

Fig. 9. The integral dose distribution for pion beams at different points of the depth dose distribution:

o at the peak of the depth-dose distribution for a pure π^- beam,

ø at the peak of the depth-dose distribution for a contaminated π^- beam,

□ halfway up the leading edge of the Bragg peak for a contaminated π^- beam,

□ halfway down the trailing edge of the Bragg peak for a contaminated π^- beam,

△ at the peak of the depth-dose distribution for a contaminated π^+ beam.

Fig. 10. Isodose distribution of a 65-MeV π^+ beam (contaminated).

Fig. 11. Isodose distribution of a 65-MeV π^+ beam (pure).

Fig. 12. Isodose distribution of a 65-MeV π^- beam (contaminated).

Fig. 13. Isodose distribution of a 65-MeV π^- beam (pure).

Fig. 14. Depth dose distribution of 67-MeV and 91-MeV π^- beams in Lucite:

o pure,

△ contaminated.

Fig. 15. Differential range curves for 67-MeV and 91-MeV π^- beams, obtained by using plastic scintillators.

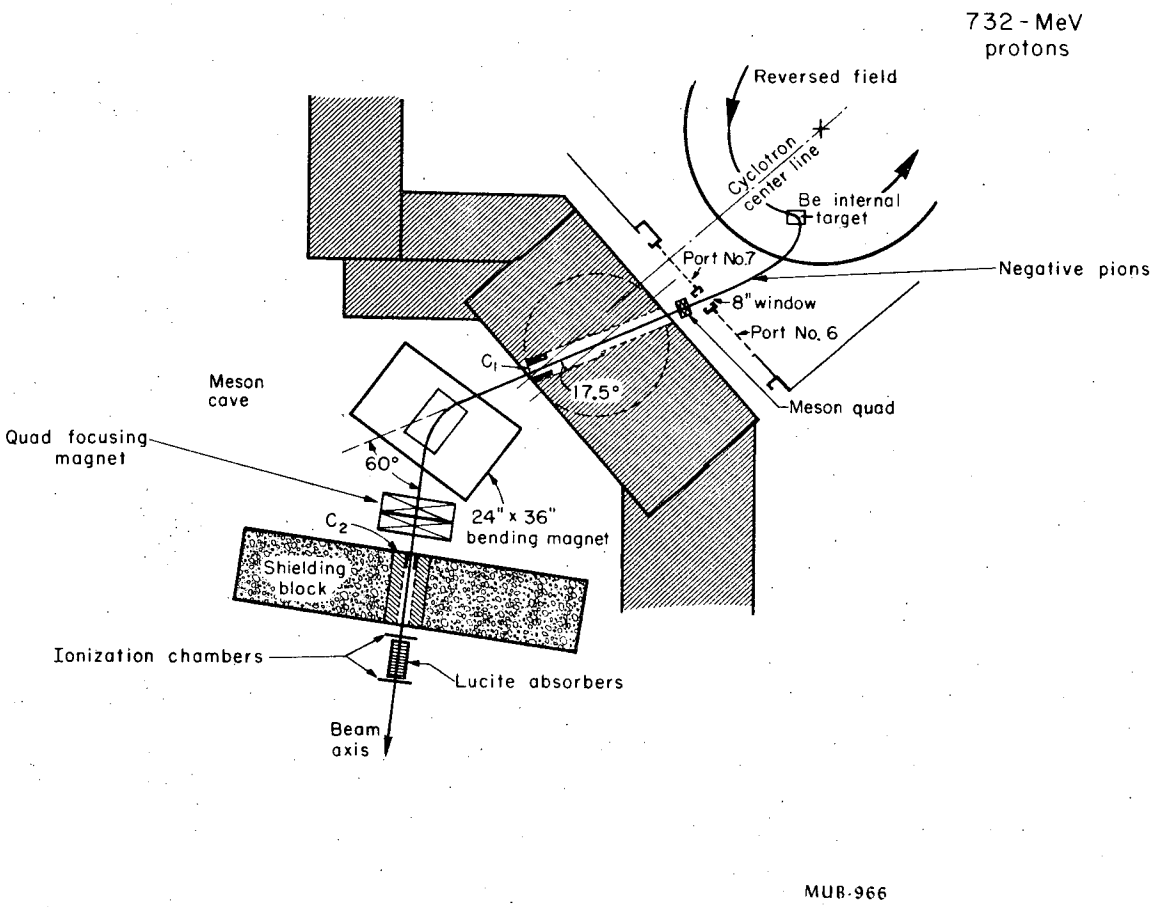
732 - MeV
protons
Reversed field
Cyclotron
center line
Be internal
target
Port No.7
Negative pions
8" window
Port No. 6
Meson quad
C_1
17.5°
Meson
cave
Quad focusing
magnet
60°
24" x 36"
bending magnet
C_2
Shielding
block
Ionization chambers
Lucite absorbers
Beam
axis
MUB-966

Fig. 1

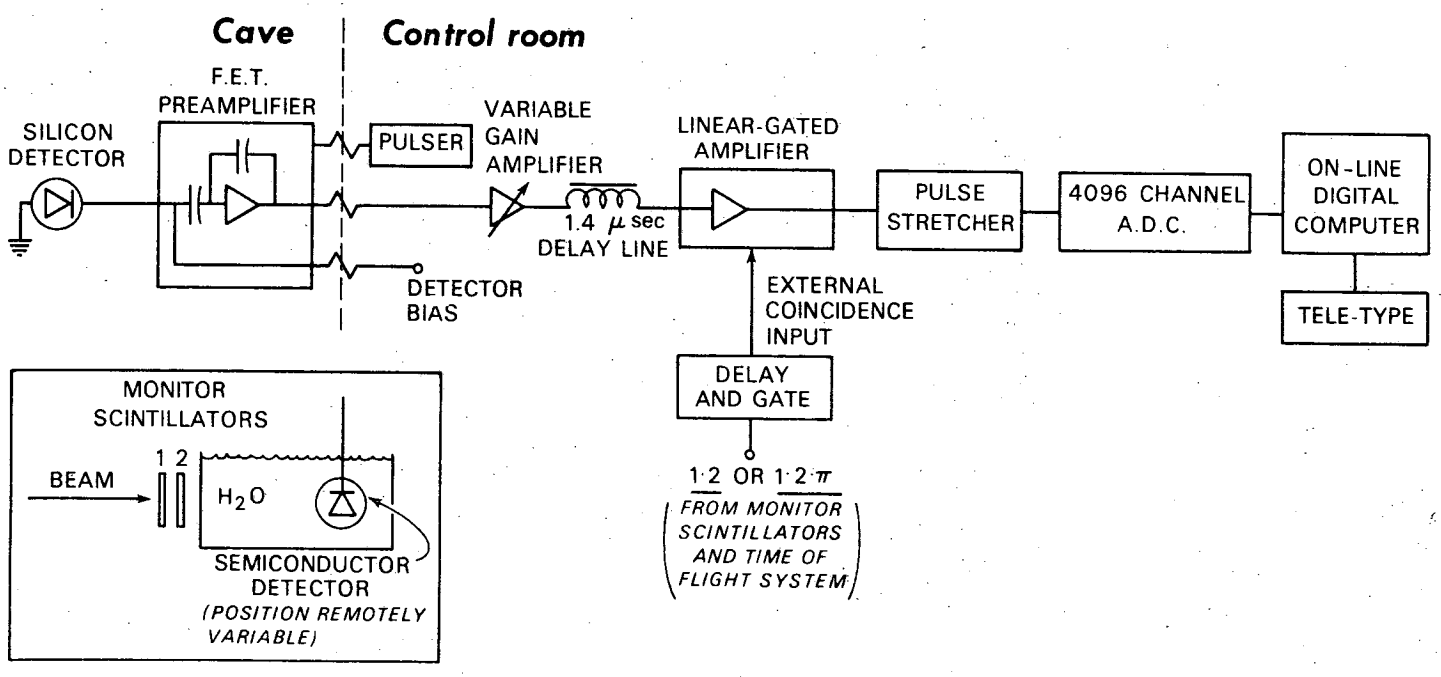

DBL 678-1730

Fig. 2

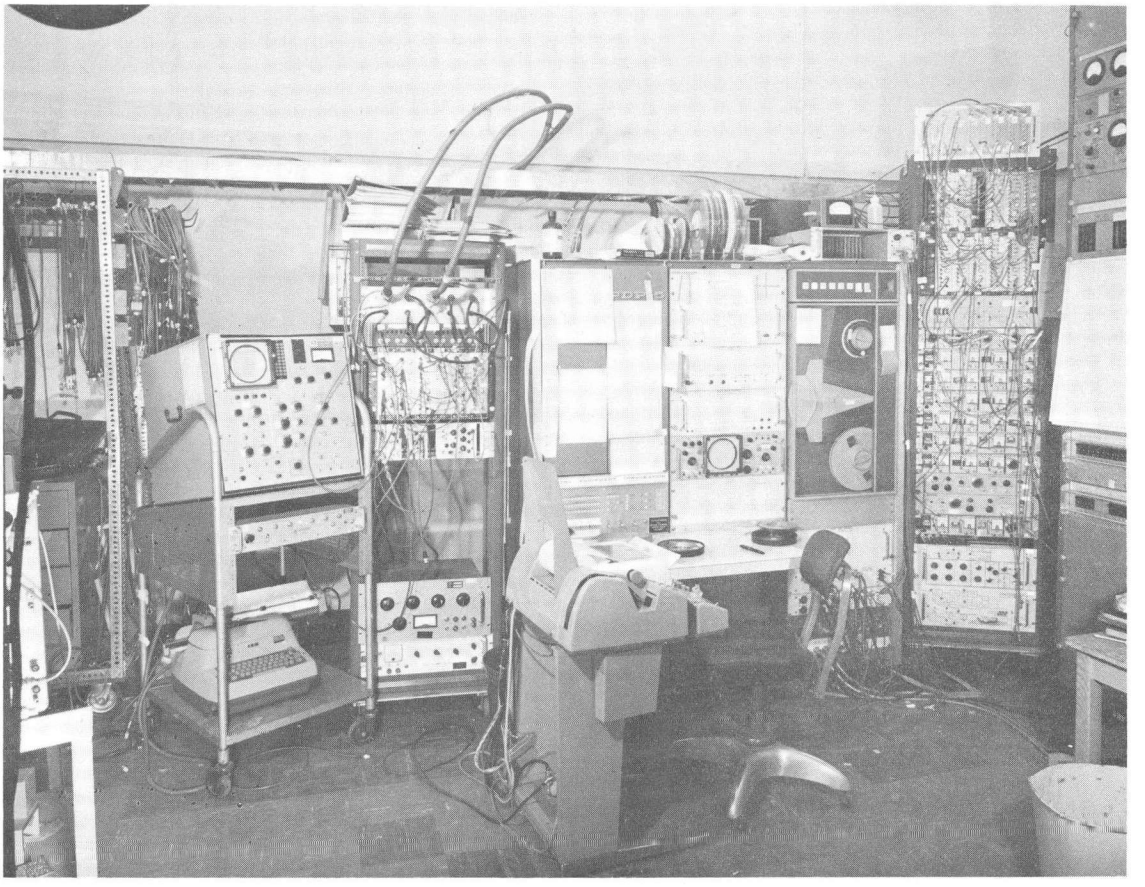

XBB 675-2519

Fig. 3

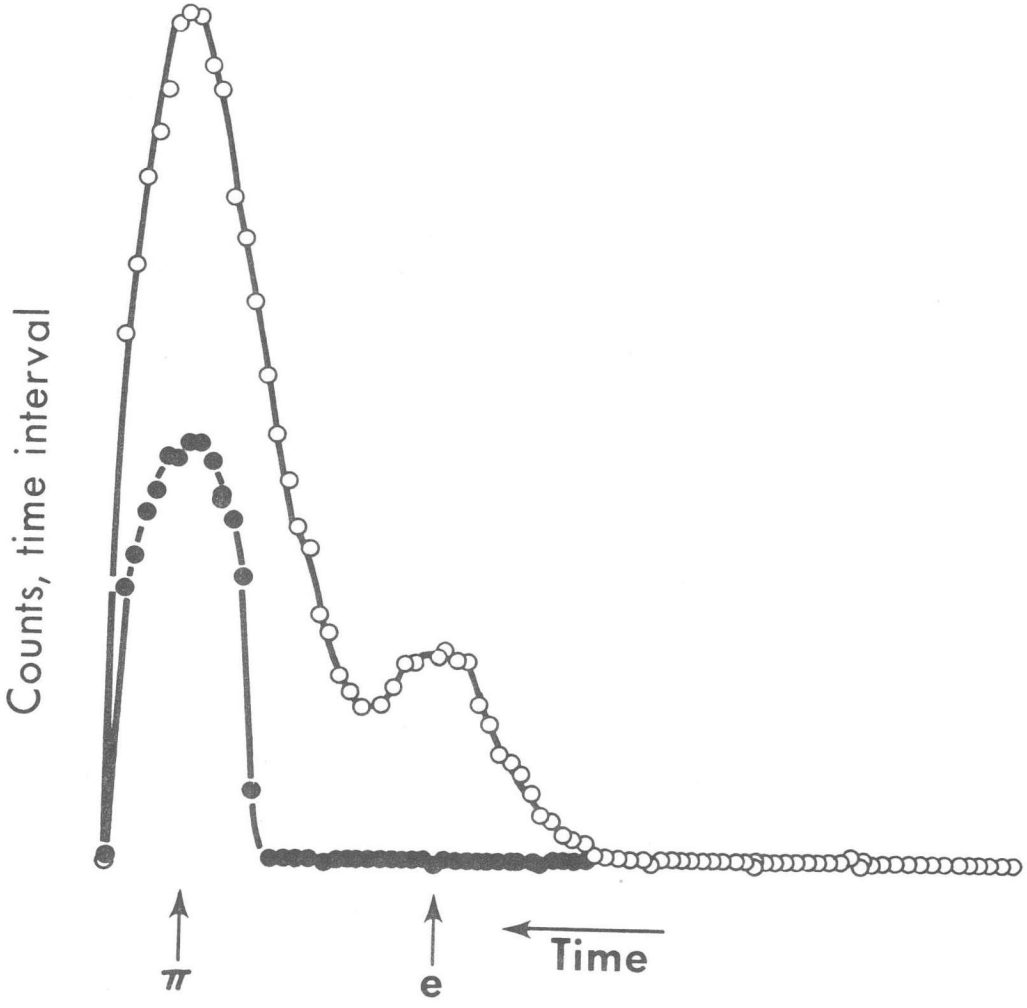

DBL 677-1696

Fig. 4

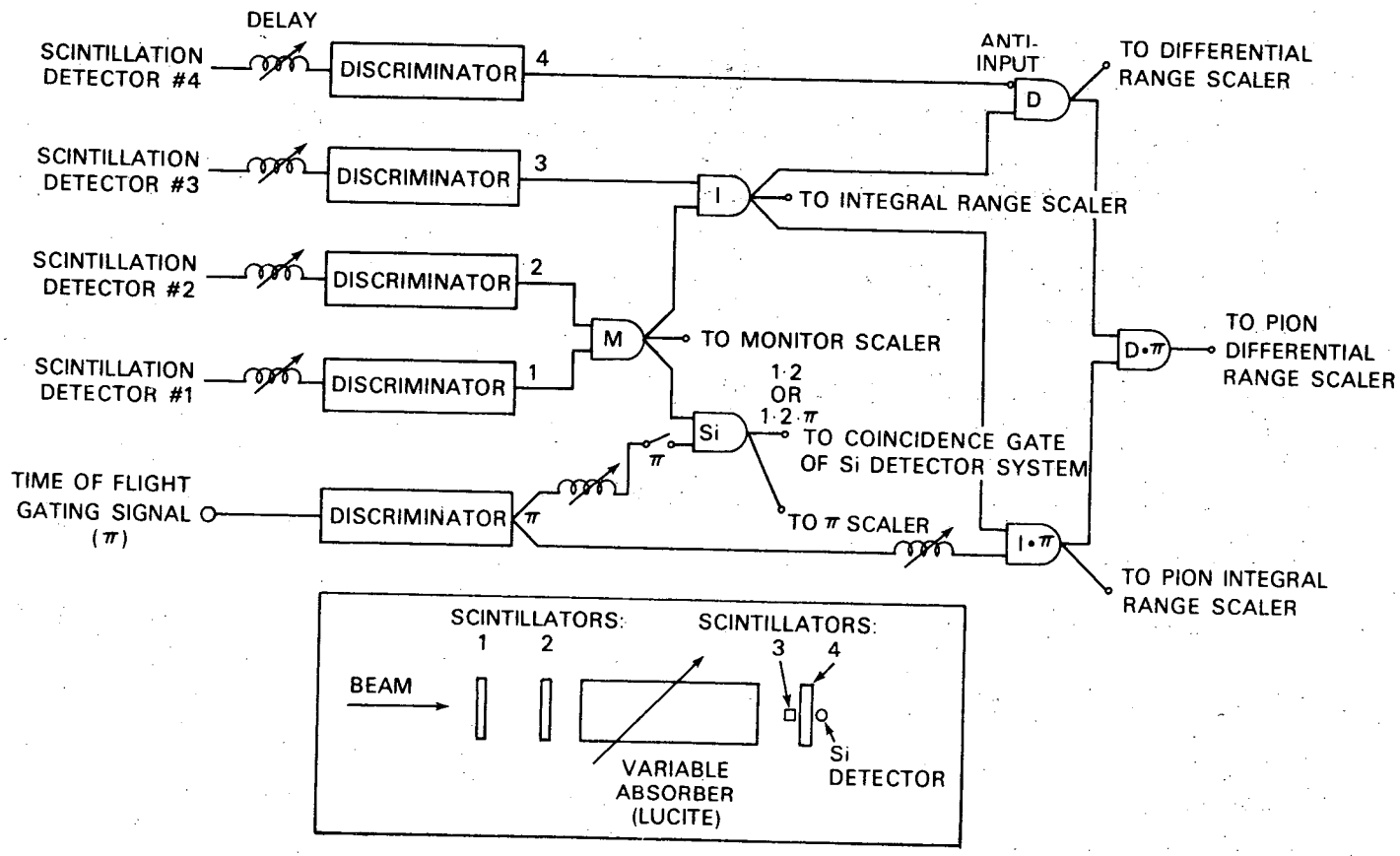

DBL 678-1729

Fig. 5

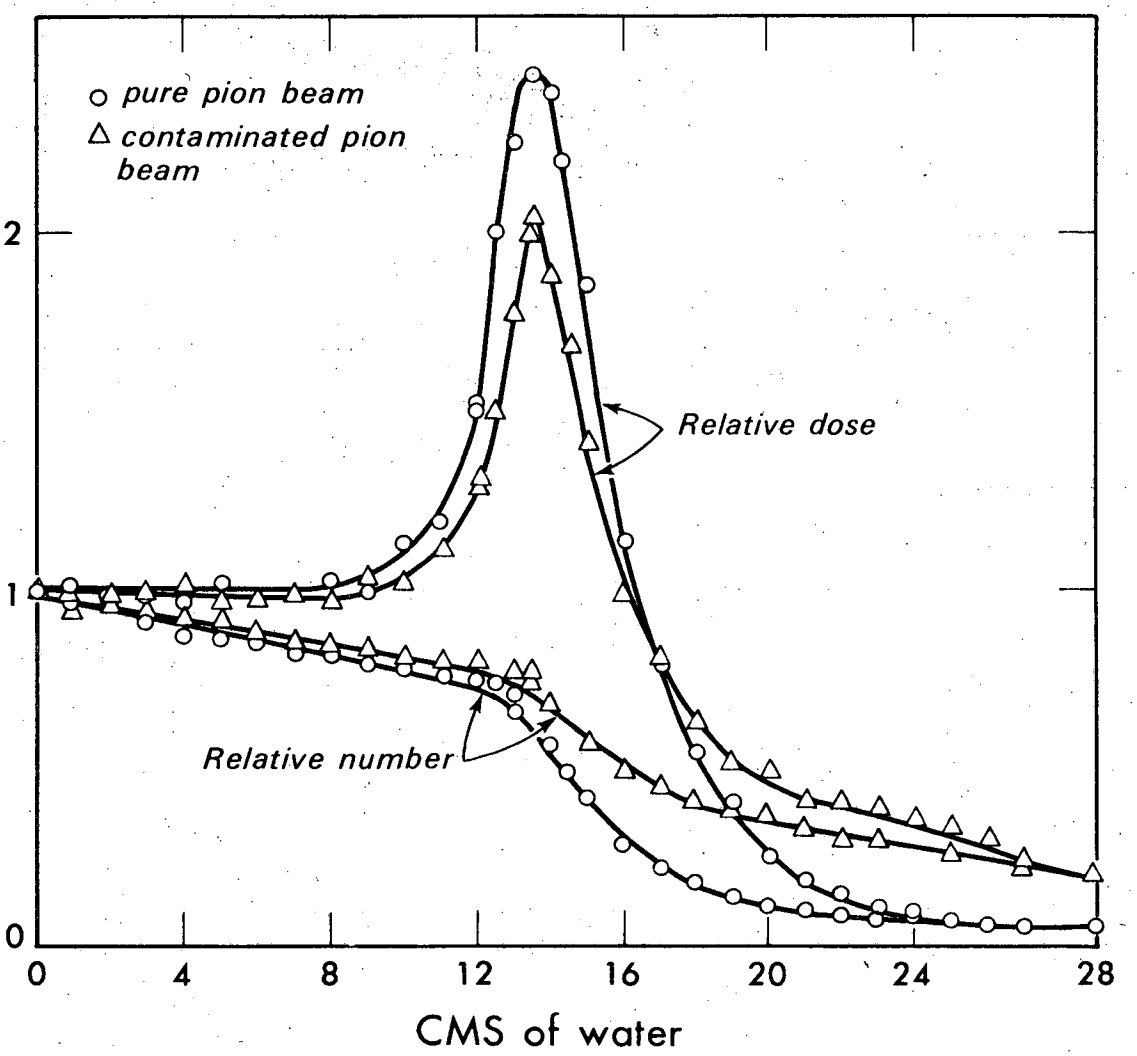
pure pion beam
contaminated pion beam
Relative dose
Relative number
2
1
0
0
4
8
12
16
20
24
28
CMS of water
DBL 677-1700

Fig. 6

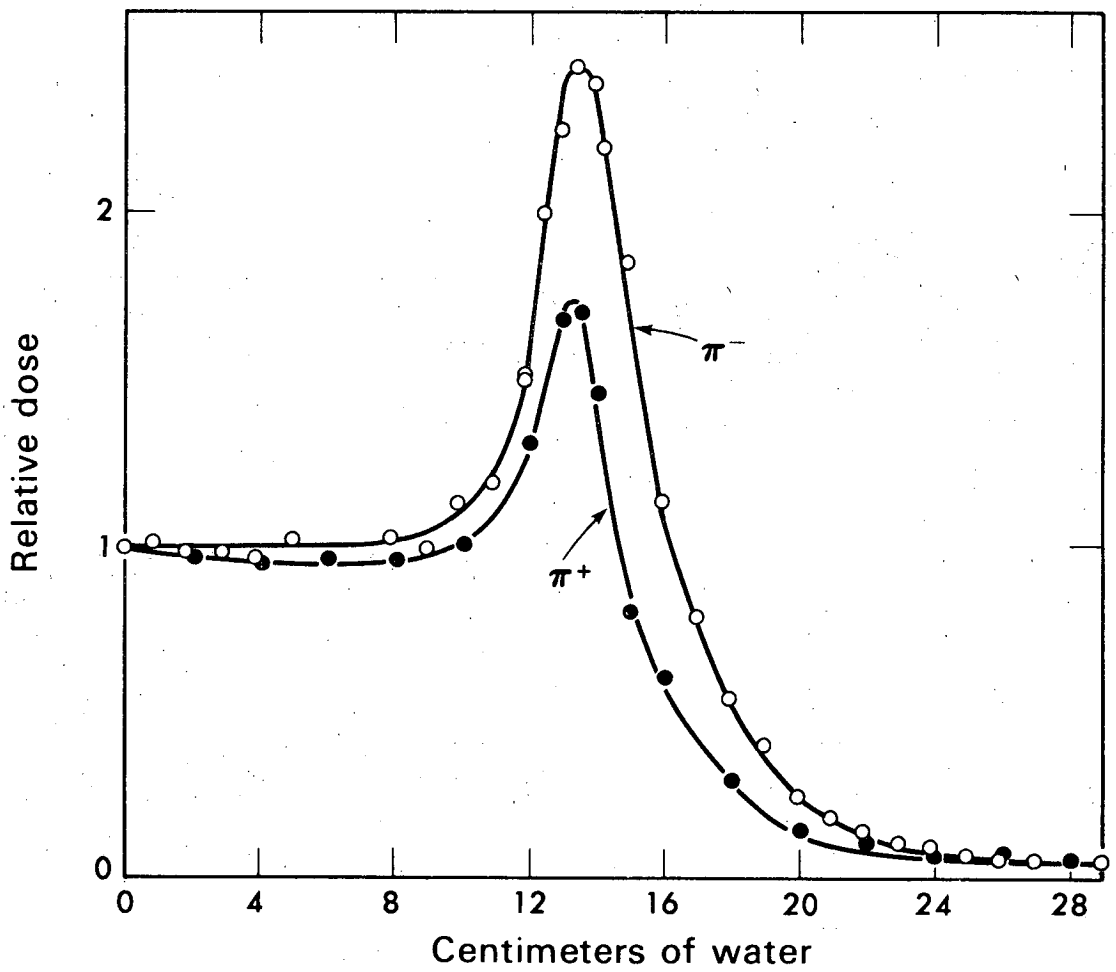

DBL 677-1698

Fig. 7

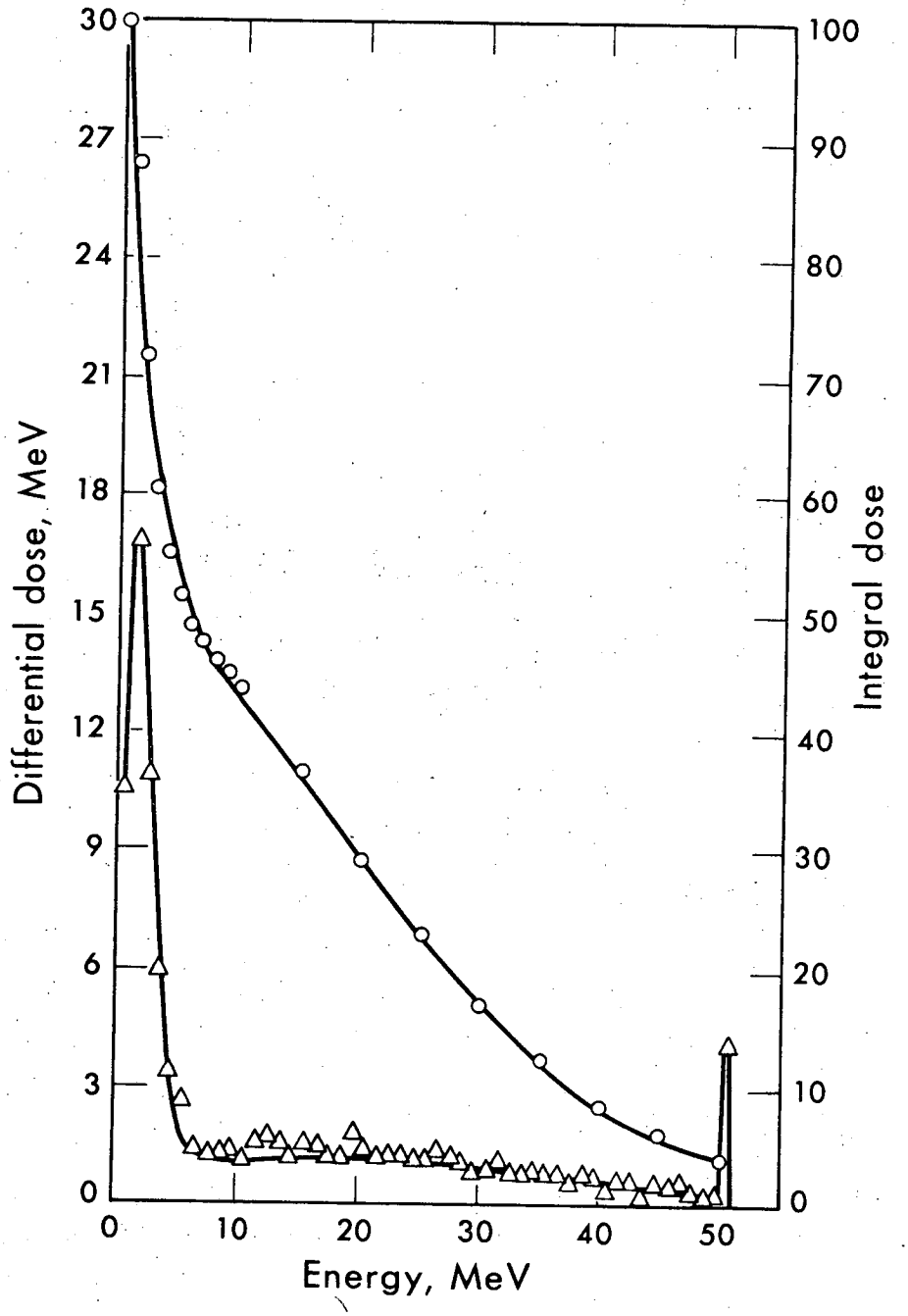
Differential dose, MeV
Integral dose
Energy, MeV
0
3
6
9
12
15
18
21
24
27
30
0
10
20
30
40
50
0
10
20
30
40
50
60
70
80
90
100
DBL 677-1701

Fig. 8

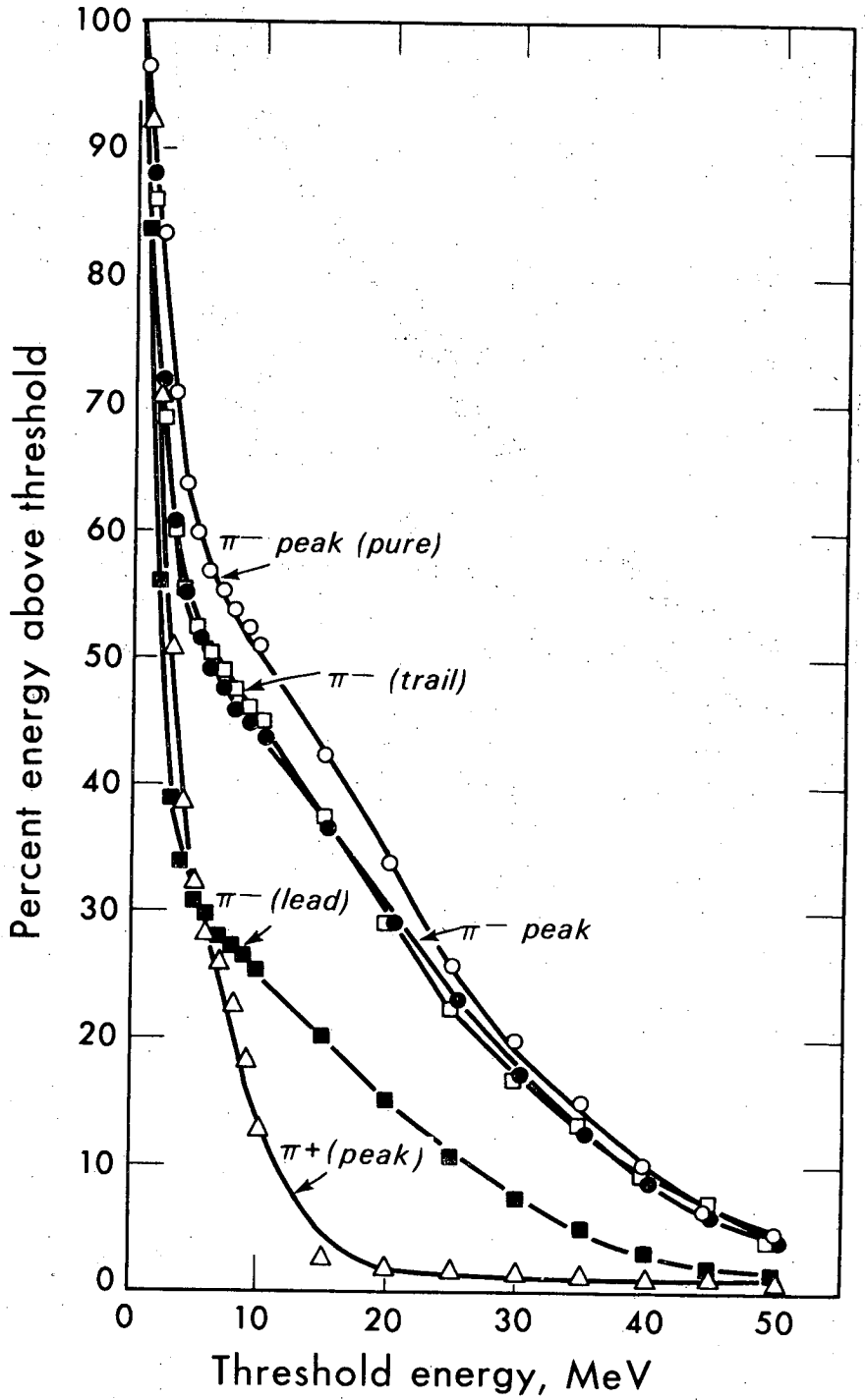
Percent energy above threshold
Threshold energy, MeV
0
10
20
30
40
50
60
70
80
90
100
π− peak (pure)
π− (trail)
π− (lead)
π− peak
π+ (peak)
DBL 677-1697

Fig. 9

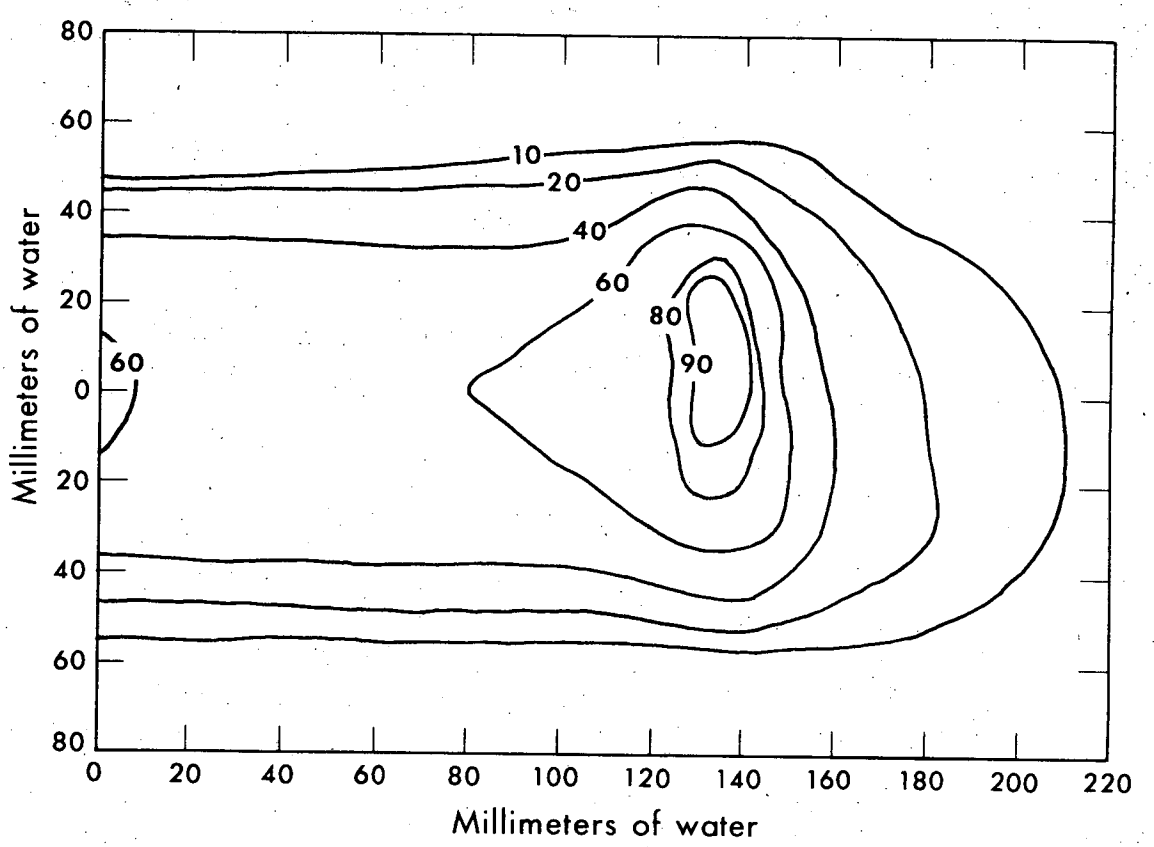
80
60
40
20
0
20
40
60
80
Millimeters of water
10
20
40
60
80
90
60
0
20
40
60
80
100
120
140
160
180
200
220
Millimeters of water
DBL 677-1702

Fig. 10

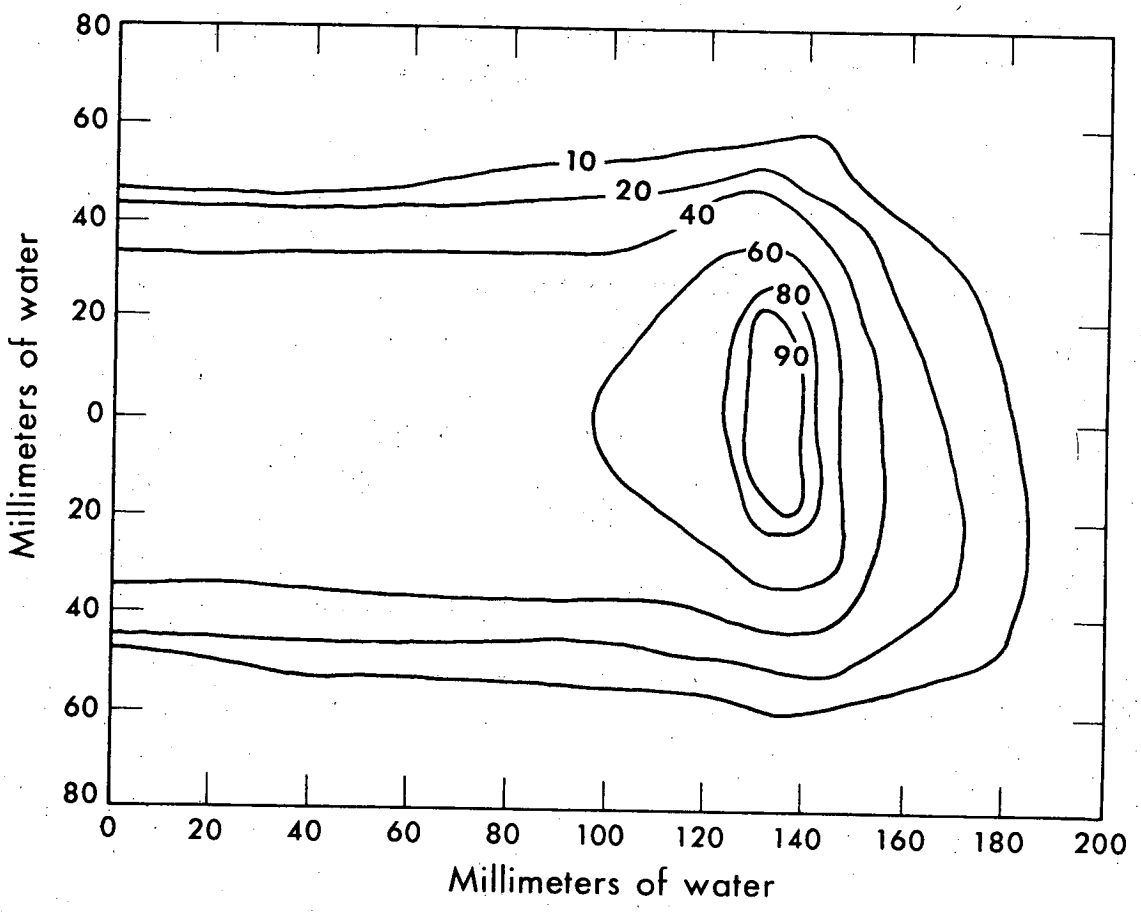

DBL 677-1703

Fig. 11

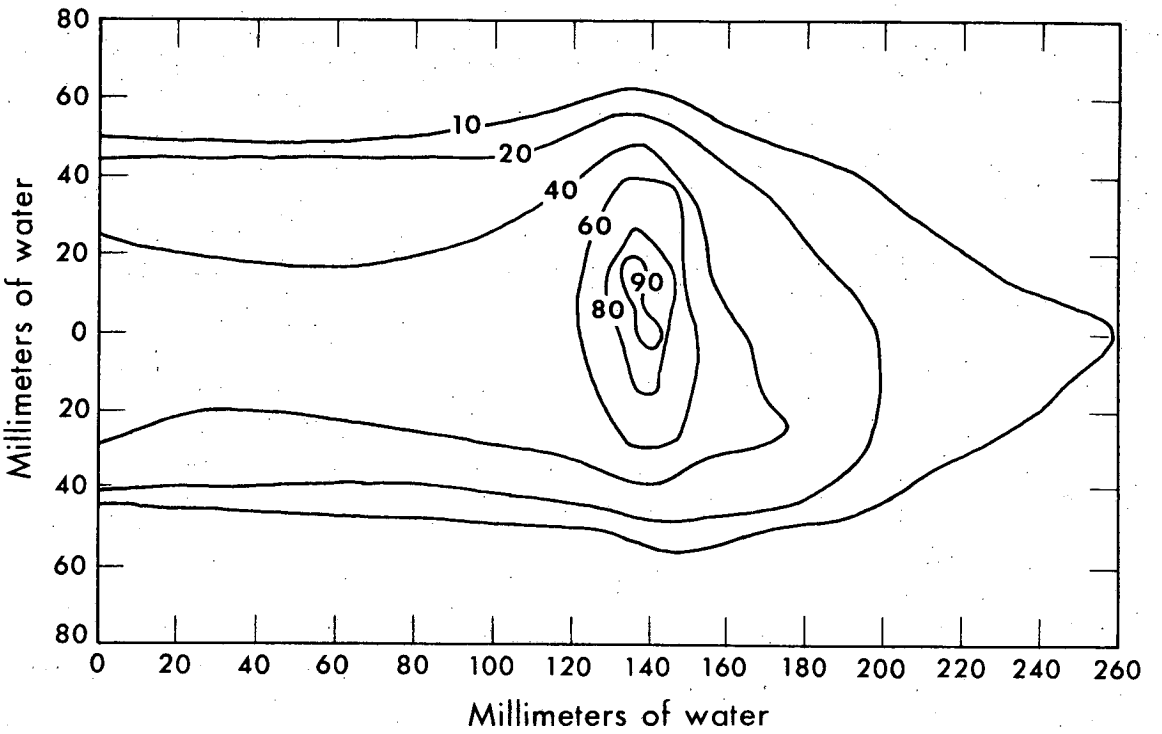

DBL 677-1705

Fig. 12

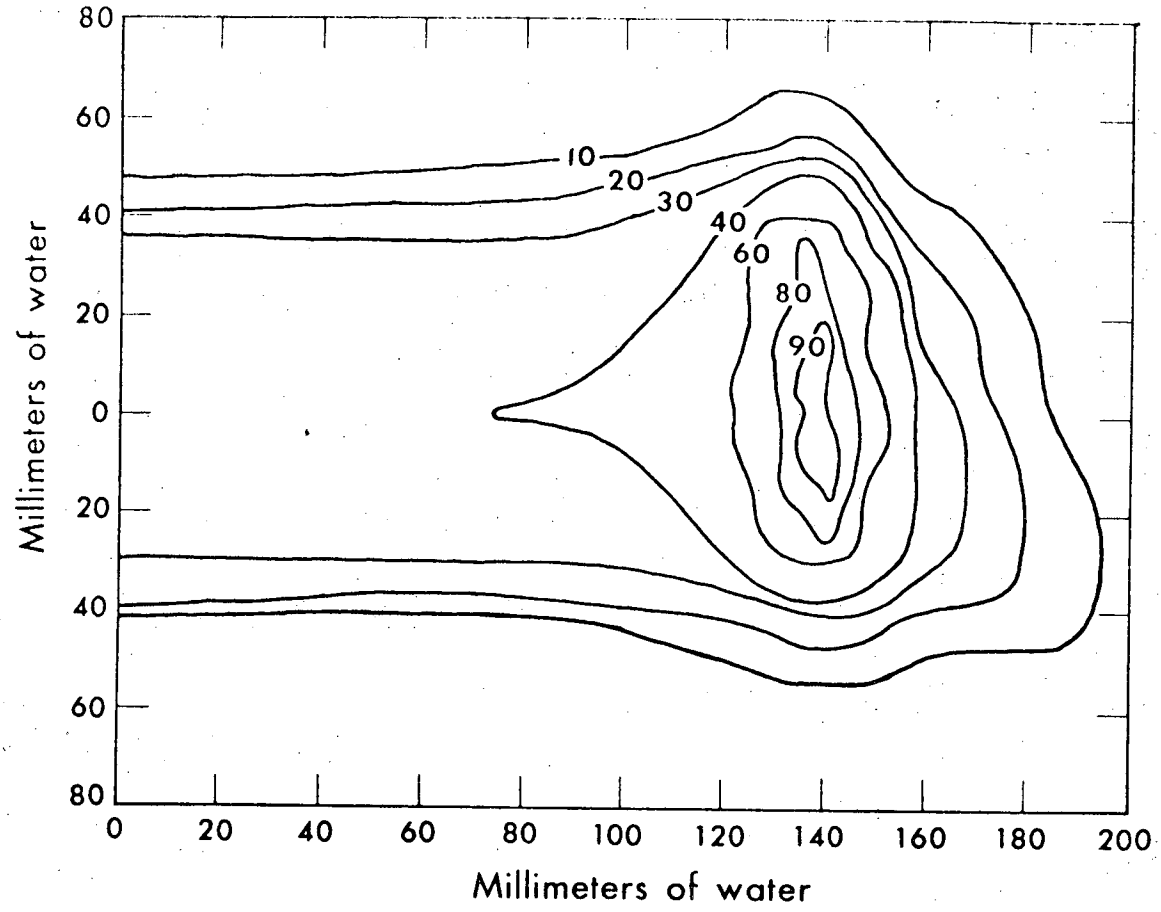

DBL 677-1704

Fig. 13

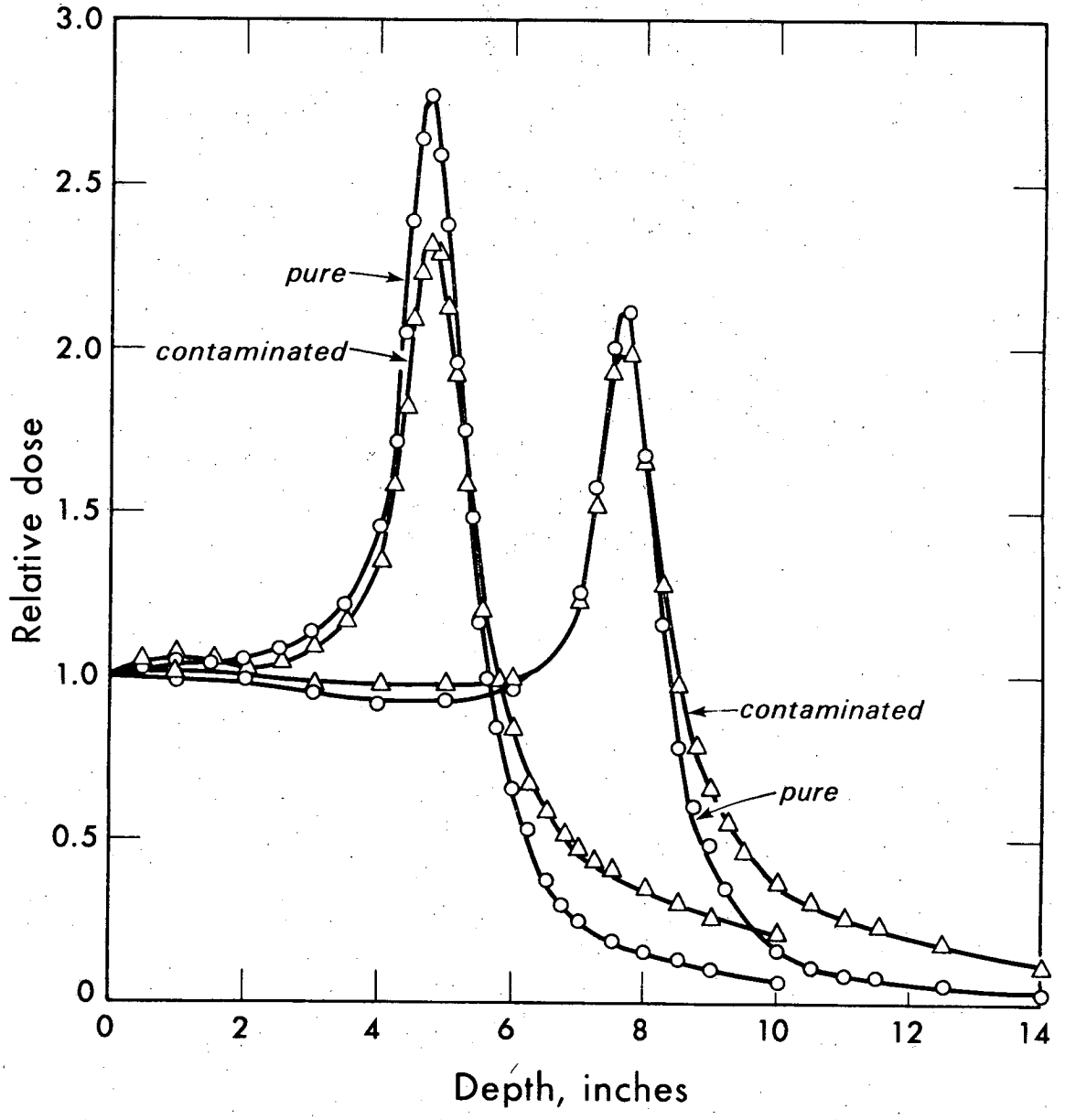

DBL 677-1699

Fig. 14

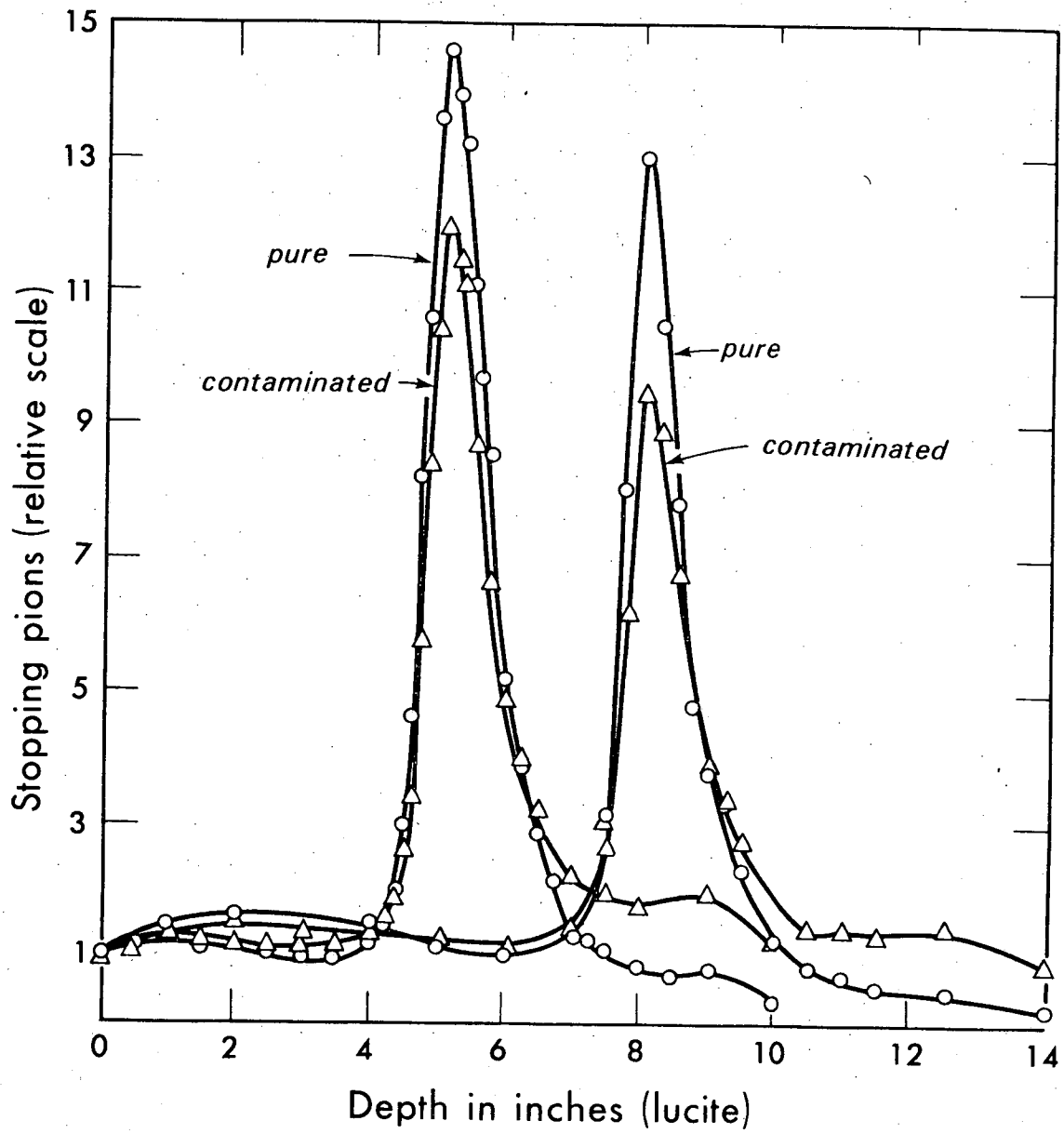

DBL 677-1706

Fig. 15

LEGAL NOTICE

TECHNICAL INFORMATION DIVISION
LAWRENCE RADIATION LABORATORY
UNIVERSITY OF CALIFORNIA
BERKELEY, CALIFORNIA 94720